CONF-881125--7

BNL-42409

Proceeding of the Rare Decay Syposium in Vancouver, 1988

Search for $K^+ \to \pi^+ \nu\bar{\nu}$

BNL--42409

DE89 010251

- E787 collaboration -

M.S. Atiya, I-H. Chiang, J.S. Frank, J.S. Haggerty, M. Ito,
T.F. Kycia, K.K. Li, L.S. Littenberg, A.J. Stevens, and R.C. Strand

Brookhaven National Laboratory, Upton, N.Y. 11973

W.C. Louis

Los Alamos National Laboratory, Los Alamos, NM 87545

D.S. Akerib, D.R. Marlow, P.D. Meyers,
M.A. Selen, F.C. Shoemaker and A.J.S. Smith

Physics Department, Princeton University, Princeton, NJ 08544

G. Azuelos, E.W. Blackmore, D.A. Bryman, L. Felawka,
P. Kitching, Y. Kuno, J.A. Macdonald, T. Numao,
P. Padley, J-M. Poutissou and J. Roy

TRIUMF, Vancouver, BC, Canada V6T 2A3

R. Poutissou

Université de Montréal, Montréal, Québec, Canada H3C 3J7

(presented by Y. Kuno)

ABSTRACT: A description of the detector and present status of an experiment to search for the decay $K^+ \to \pi^+ \nu\bar{\nu}$ at Brookhaven National Laboratory is presented.

1. INTRODUCTION

A search for the decay $K^+ \to \pi^+ \nu\bar{\nu}$ is being undertaken in Experiment 787 at Brookhaven National Laboratory. This rare decay mode is mediated by flavor changing neutral currents, forbidden in first-order by the GIM mechanism, and occurs only in higher-order diagrams in accordance with the standard model of the electroweak interaction.[1] So far the predictions of the standard model agree

DISTRIBUTION OF THIS DOCUMENT IS UNLIMITED

well with the experimental results up to the level of first-order interactions. Therefore, a precise test of the standard model at higher-orders is strongly desirable. Suppressed decays such as $K^+ \to \pi^+ \nu\bar{\nu}$ are sensitive to higher-order interactions because there are only small contributions of "long distance effects". The second-order diagrams in $K^0 - \bar{K}^0$ mixing and $K_L^0 \to \mu^+\mu^-$, in contrast, suffer large long distance effects (either electromagnetic or hadronic) which introduce large ambiguities. Therefore, the search for the decay $K^+ \to \pi^+ \nu\bar{\nu}$ provides a comparatively clean test of the second-order weak interaction. [2)]

The second-order diagrams for $K^+ \to \pi^+ \nu\bar{\nu}$ are in Fig.1, showing two intermediate weak vector bosons involved in the loop. The calculated branching ratio of $K^+ \to \pi^+ \nu\bar{\nu}$ [3-8)] is given per the lepton flavor by

$$B(K^+ \to \pi^+ \nu_i \bar{\nu_i}) = \frac{0.61 \times 10^{-6}}{|V_{us}|^2} |\sum_{j=c,t} V_{js}^* V_{jd} D(x_j)|^2 \qquad (1)$$

where $D(x_j)$ is a function of $x_j = (m_j/m_w)^2$, m_j and m_w are the mass of the charge 2/3 quarks and of the intermediate weak vector boson, respectively. V_{ij} is

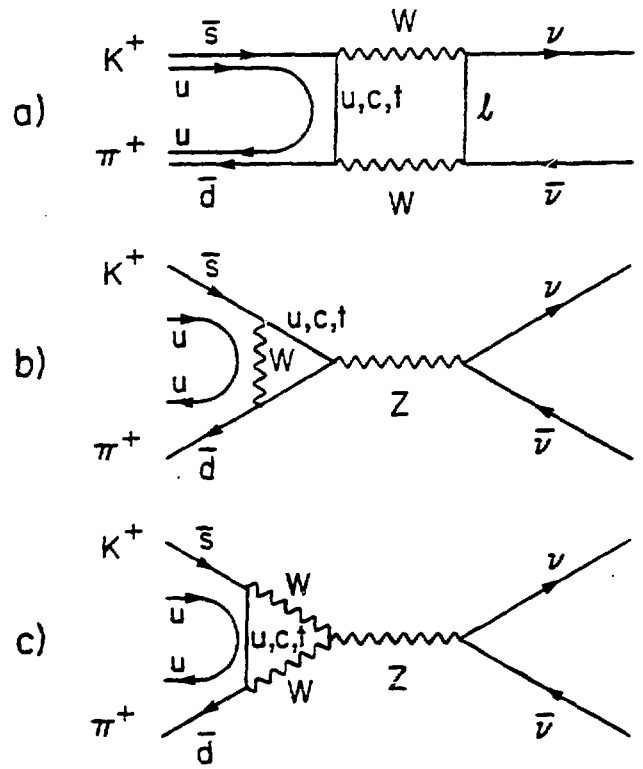

Fig.1 Second-order diagrams for $K^+ \to \pi^+ \nu\bar{\nu}$.

the Kobayashi-Maskawa (K−M) matrix [9] given by

$$V_{ij} = \begin{pmatrix} V_{ud} & V_{us} & V_{ub} \\ V_{cd} & V_{cs} & V_{cb} \\ V_{td} & V_{ts} & V_{tb} \end{pmatrix} = \begin{pmatrix} c_1 & s_1 c_3 & s_1 s_3 \\ -s_1 c_2 & c_1 c_2 c_3 - s_2 s_3 e^{i\delta} & c_1 c_2 s_3 + s_2 c_3 e^{i\delta} \\ -s_1 s_2 & c_1 s_2 c_3 + c_2 s_3 e^{i\delta} & c_1 s_2 s_3 - c_2 c_3 e^{i\delta} \end{pmatrix} \quad (2)$$

where c_i, s_i are $\cos\theta_i$, $\sin\theta_i$ respectively of the K−M mixing angle θ_i and δ is the CP violating phase. For small K−M mixing angle, the branching ratio is approximated by

$$B(K^+ \to \pi^+ \nu_i \overline{\nu_i}) = 0.61 \times 10^{-6} |D(x_c) + s_2(s_2 + s_3 e^{i\delta}) D(x_t)|^2 \quad (3)$$

The second term in eq.(3) is expected to dominate owing to the heavy mass of the *top* quark. As a result, the branching ratio of $K^+ \to \pi^+ \nu\overline{\nu}$ is very sensitive to the K−M matrix elements, especially s_2 and s_3, as well as to the mass of the *top* quark. Recently, using the observed large $B_d^0 - \bar{B}_d^0$ mixing [10], the B meson lifetime τ_b [11] and $\Gamma(b \to u)/\Gamma(b \to c)$ [12], s_2 and s_3 were evaluated and the branching ratio of $K^+ \to \pi^+ \nu\overline{\nu}$ was predicted.[8] In Fig.2, the limit of the branching ratio for the three lepton generations is shown to be in the range $(1 - 8) \times 10^{-10}$ depending on the *top* quark mass. The proposed goal of the experiment is just in the range of the prediction of the standard model. This prediction can be improved if the K−M matrix elements are better known or the *top* quark is found. Conversely, a signal for $K^+ \to \pi^+ \nu\overline{\nu}$ in the predicted region will give constraints on the K−M matrix elements and the *top* quark mass. In particular, V_{td} (or s_2), one of the smallest K−M matrix elements, could be determined more precisely than from the $B_d^0 - \bar{B}_d^0$ mixing which has also an ambiguity arising from the hadronic matrix elements.

The observation of $K^+ \to \pi^+ \nu\overline{\nu}$ well above the prediction will indicate new physics beyond the standard model. The possibilities include (1) extra lepton generations[6,13], (2) extra quark generations[14] or (3) existence of a light weakly-interacting neutral particle or particles. Hypothetical candidates would be super-symmetric particles[6,15] (photino, shiggs, etc.), the familon[16] which arises from flavor-symmetry breaking, the axion[17], the majoron[18], or the hyperphoton[19].

The present experimental upper limit for $K^+ \to \pi^+ \nu\overline{\nu}$ is $B(K^+ \to \pi^+ \nu\overline{\nu}) < 1.4 \times 10^{-7}$. [20] There is a large window of three orders of magnitude to search for new physics between the current limit and the prediction of the standard model.

Other decay modes can also be sought by the E787 experiment such as $K^+ \to \pi^+ \mu^+ \mu^-$ and $K^+ \to \pi^+ \gamma\gamma$. These decay modes are electromagnetically induced weak processes where long distance effects dominate. In general, understanding of long distance effects is very important in order to extract the genuine effect of the weak interaction from rare K decay experiments. Recently, there has been theoretical progress using chiral perturbation theory.[21−23] The study of the

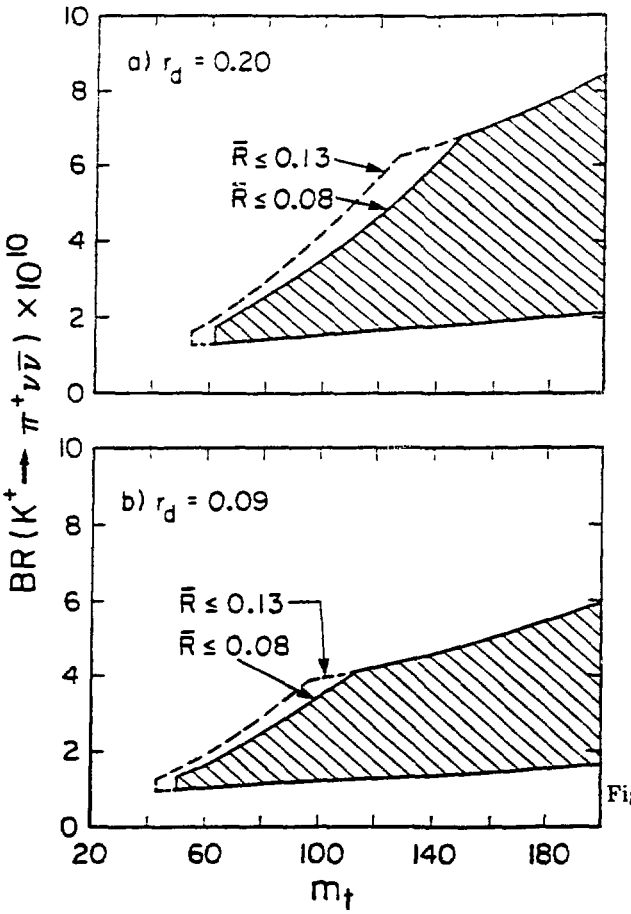

Fig.2 Limit of the prediction of the standard model, shown by the shaded area, as a function of the top quark mass.

decay modes of $K^+ \to \pi^+\mu^+\mu^-$ and $K^+ \to \pi^+\gamma\gamma$ will provide important information on the test of this theoretical framework.

The present experimental limits on the branching ratios are $B(K^+ \to \pi^+\mu^+\mu^-) \leq 2.4 \times 10^{-6}$ [24] and $B(K^+ \to \pi^+\gamma\gamma) \leq 8.6 \times 10^{-6}$ [25]. Chiral perturbation theory predicts $B(K^+ \to \pi^+\mu^+\mu^-) = (3-8) \times 10^{-8}$ [21] and $B(K^+ \to \pi^+\gamma\gamma) \geq 4 \times 10^{-7}$ [22]. Both predictions are thus within the range reachable by E787. Furthermore, the measurement of the branching ratio of $K^+ \to \pi^+\gamma\gamma$ is important because it could be a background for $K^+ \to \pi^+\nu\bar{\nu}$ if the photons are missed in the detector.

The decay $K^+ \to \pi^+\mu^+\mu^-$ is a valid hunting ground for a light Higgs boson, H, in the decay of $K^+ \to \pi^+ H$. Since the coupling of the Higgs to a fermion is proportional to the fermion mass, the decay $H \to \mu^+\mu^-$ dominates in the mass region between $2m_\mu < M_H < 2m_\pi$. The decay of the Higgs is also calculated to be fast enough to be detectable. According to various theoretical estimates[26], the

present experimental limit cannot exclude the existence of the light Higgs boson in this mass range.

By tagging with the π^+ from the decay $K^+ \rightarrow \pi^+\pi^0$, the E787 experiment can also study the rare decay of $\pi^0 \rightarrow xx'$, where x, x' are non-interacting particles.

2. DETECTOR

The signature of $K^+ \rightarrow \pi^+\nu\bar{\nu}$ is a single π^+ unaccompanied by other signals (i.e. $K^+ \rightarrow \pi^+ +$"*nothing*"). Since the π^+ spectrum for $K^+ \rightarrow \pi^+\nu\bar{\nu}$ is not discrete, other dominant decay-modes overlap the region of $K^+ \rightarrow \pi^+\nu\bar{\nu}$ and could be sources of background. Fig.3 shows the expected spectra of the range and momentum for $K^+ \rightarrow \pi^+\nu\bar{\nu}$ along with the other decay modes. The decays $K^+ \rightarrow \mu^+\nu$ ($K_{\mu 2}$) and $K^+ \rightarrow \pi^+\pi^0$ ($K_{\pi 2}$) are the two largest potential backgrounds. They could mimic the $K^+ \rightarrow \pi^+\nu\bar{\nu}$ signals if the muon is misidentified as a pion in $K_{\mu 2}$ or if the photons from the π^0 decay are undetected in $K_{\pi 2}$. In order to minimize the background, only the 20% of the total spectrum in the kinematic region above the monoenergetic peak of $K_{\pi 2}$ (momentum $P(\pi^+) > 205$ MeV/c) is considered.

Even in the selected kinematic region, a lower momentum tail from the $K_{\mu 2}$ peak or a higher momentum tail from the $K_{\pi 2}$ peak can contribute background events. Therefore, important characteristics of the detector to reduce backgrounds are (1) *excellent π/μ particle identification* and (2) *efficient photon detection capability*. For particle identification, the range, momentum and kinetic energy of

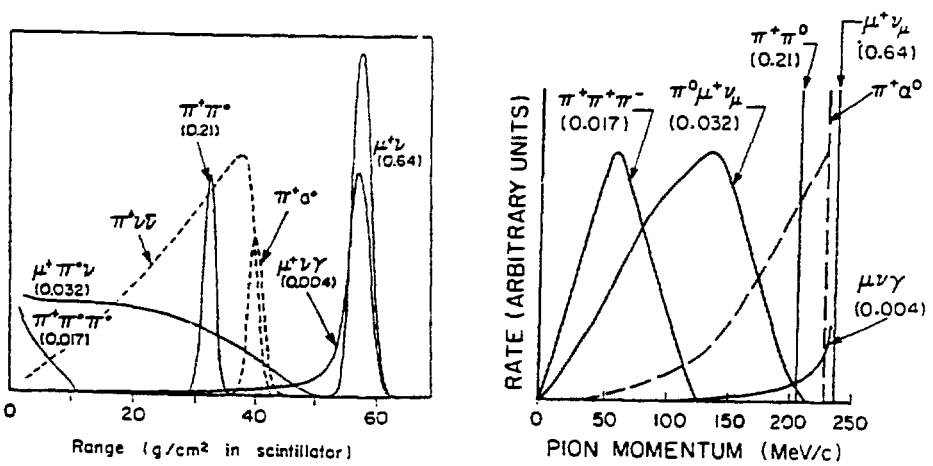

Fig.3 Range and momentum spectra of $K^+ \rightarrow \pi^+\nu\bar{\nu}$ and background decays.

charged decay products are measured and their correlations are exploited to distinguish pions from muons. In order to enable precise measurements of these three quantities and to maximize photon veto efficiency, the geometry of K^+ decay at rest was selected. In addition to the correlation of range/momentum/energy for π/μ particle identification, the characteristic decay sequence of $\pi^+ \rightarrow \mu^+ \rightarrow e^+$ is observed. The photon detection system, consisting of lead-scintillator sandwich, covers nearly 4π of solid angle.

Other potential background decay-modes appearing in the kinematic region of interest are $K^+ \rightarrow \mu^+\nu\gamma$, $K^+ \rightarrow \mu^+\pi^0\nu$ ($K_{\mu 3}$) and $K^+ \rightarrow \pi^+\gamma\gamma$, etc. which can be rejected by a combination of the π/μ particle identification and the photon veto. The other possible background sources are beam pions scattering into the detector following K^+ stops, or K^+ charge exchange reactions, etc. In order to reduce these kinds of backgrounds, the beam counters have efficient K^+ beam identification and high rejection capability for secondary incident particles from the beam line, and an active highly-segmented scintillation-fiber target system is used to track the K^+'s and the π^+'s.

A schematic side view of the detector is shown in Fig.4. It has an acceptance of 2π for π^+ detection. Incoming kaons are stopped in the target located at the center of the detector, and pions from K^+ decay are momentum-analyzed as they pass through a cylindrical drift chamber and are stopped in a stack of scintillators (range stack) which measures the range and kinetic energy of the pions. The decay sequence of $\pi^+ \rightarrow \mu^+ \rightarrow e^+$ is measured using transient digitizers on the range stack phototube signals. Surrounding the range stack and drift chamber is the 4π photon detection system comprised of barrel and endcap sections. All these systems are contained in a normal solenoid magnet which produces a magnetic field of 10 kG along the beam direction. A typical online event display for $K_{\pi 2}$ is shown in Fig.5, where the pion is stopped in the range stack and the two photons from π^0 decay are detected in the barrel photon-veto system. A brief description on the E787 detector can also be found elsewhere.[27]

2.1 Beam Counter System

A 775 MeV/c kaon beam from the Low Energy mass-Separated Beam (LESB-1) at the Alternating Gradient Synchrotron (AGS) is slowed by 50 cm of BeO degrader and stopped in the scintillator target. Typical intensity of the kaon beam was about 150 k stopped K^+ per spill and the ratio of $K^+ : \pi^+$ was about 1:2.5 in the 1988 run. The kaons were selected by a differential Čerenkov counter which uses a lucite radiator. The energy deposited (dE/dx) in a 6 mm-thick scintillator located in front of the target can also be used to select kaons. The other

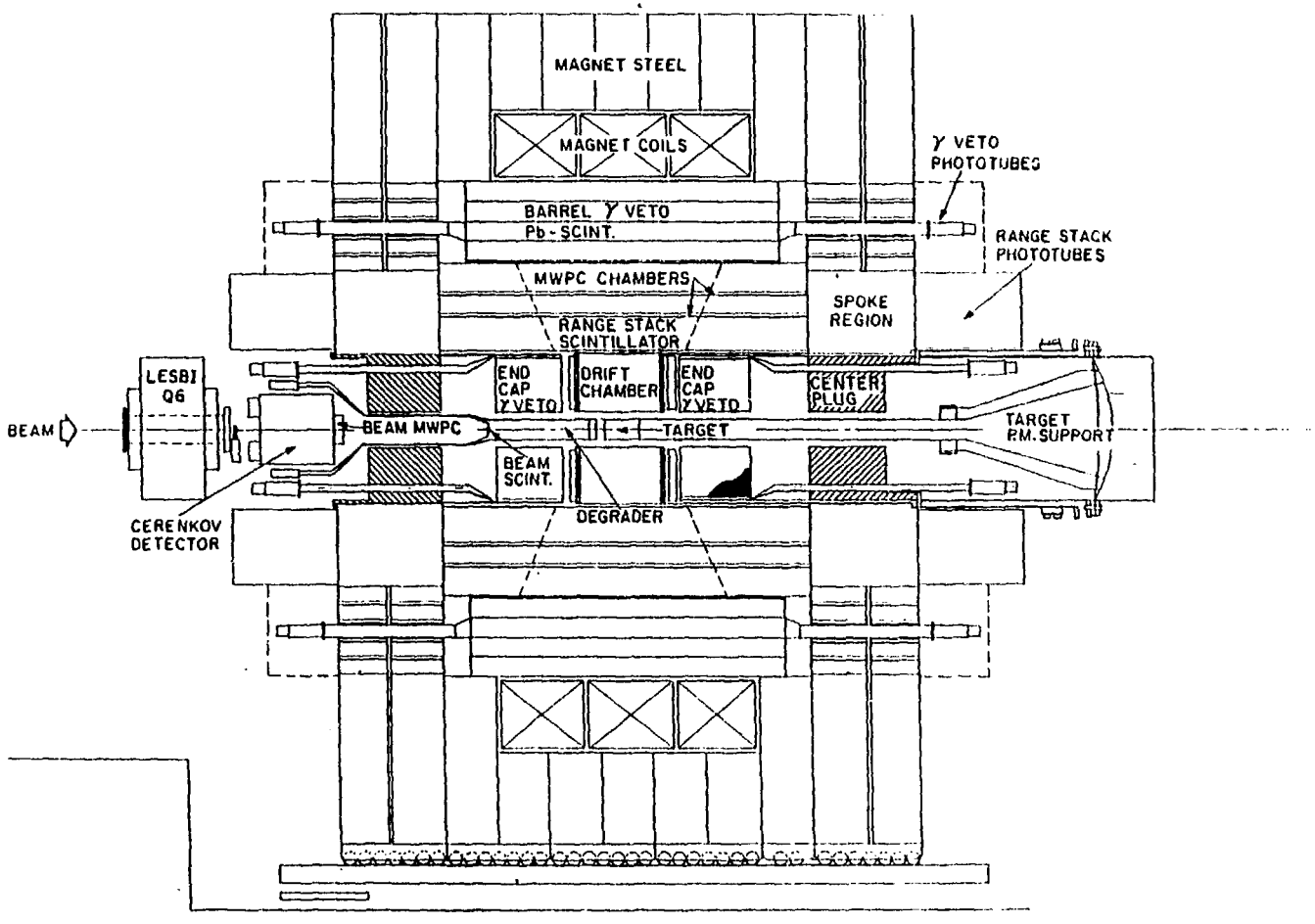

Fig.4 Schematic side view of the detector.

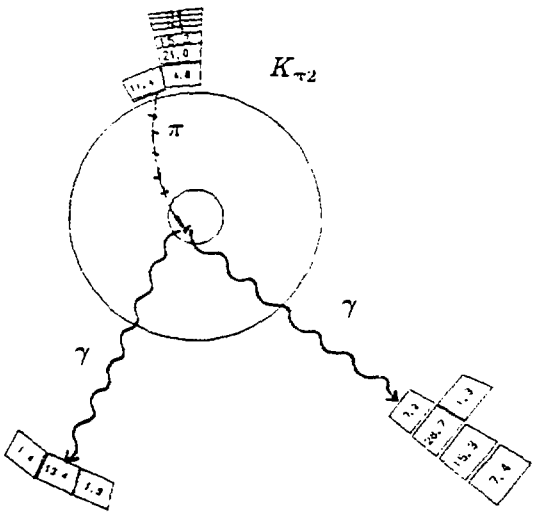

Fig.5 Display of a $K_{\pi 2}$ event showing the π^+ track and stop in the range stack and the signals of the two photons from the π^0 in the barrel photon veto.

elements of the beam counter system include a beam hodoscope and a fast multi-wire proportional chamber. They are used to monitor the beam profile as well as to identify multiple entries of beam particles into the detector. The wire chamber contains three planes in which the first plane has vertical wires and the other two have wires at $\pm 45°$ to the vertical. A gas mixture of CF_4:Isobutane=80:20 is used for fast response.

2.2 Target System

The target system[28] consists of 378 clusters of scintillation fibers. Each fiber has a round cross section with a diameter of 2 mm and is aluminum-coated. Six fibers are epoxied together to form a triangular-shaped cluster which has 75% scintillator material. The arrangement of the 378 clusters in the target is shown in Fig.6. Each cluster is viewed by a 3/8 inch photomultiplier tube (Hamamatsu R1635-02). Typical attenuation length in the scintillation fiber is about 2 m and the light output is about 5 photoelectrons per MeV. The total diameter of the target between the flat surfaces is about 10 cm. The high segmentation utilizing scintillation fibers was designed to enable measurement of the energy and range of the decay pions as well as of the energy and position of stopping K^+'s. The radial resolution of the decay vertex is $\sim$ 2mm. The segmentation also allows rejection of backgrounds in which photons convert in the target. The tracks of K^+'s and π^+'s are identified by the timing and energy information. The incident kaons have large prompt-energy deposit, typically 50 MeV, while decay pions have relatively small energy at a later time. The K^+ lifetime measured in the target is shown in Fig.7,

where the time resolution is $\sigma \sim 1$ ns. In order to reject the K^+ decay-in-flight and prompt scattering, only delayed events later than 2 ns with respect to the K^+ stop timing were valid in the triger mode of $K^+ \rightarrow \pi^+ \nu \bar{\nu}$.

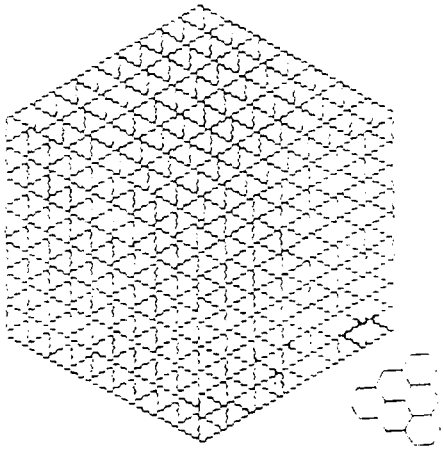

Fig.6 Crosssection of segmented scintillator fiber target.

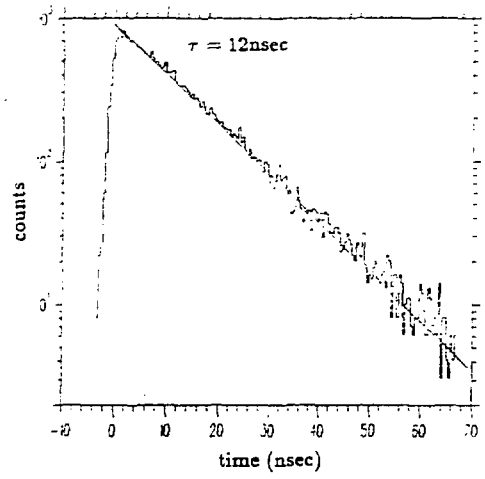

Fig.7 K decay lifetime obtained from the target.

2.3 Drift Chamber

The cylindrical drift chamber [29] is used to measure the momenta of the charged decay particles in a magnetic field of 10 kG. It occupies the volume from 11 cm to 45 cm in radius and 50 cm in length. It consists of 256 cells in 5 radial layers. The wires in layers 1, 3 and 5 are axial and those in layer 2 and 4 are at stereo with angles of $-3.5°$ and $+3.7°$, respectively. These stereo wires give information on the track positions along the axis of the drift chamber (z direction). A single cell consists of 6 instrumented sense wires of 20 μm gold-plated tungsten with wire separation of 5 mm and 19 field wires of 170 μm Be-Cu wires located at each boundary of the cell. There are two additional field wires at each end of the sense wire row. The sense wires are staggered by $\pm$ 254 μm to resolve the left-right ambiguity. A gas mixture of Argon:Ethane=50:50 with ethanol is used and a typical drift velocity is 5 cm/μsec at atmospheric pressure. The maximum drift time is about 300 ns. In a magnetic field of 10 kG, the Lorentz angle is about 25°. The position resolution of the hits in the plane perpendicular to the beam axis (xy plane) is about 150 μm at the middle of the cell; the z position resolution of the hits obtained from the stereo wires is about 2.5 mm.

2.4 Range Stack

Pions passing through the drift chamber are stopped in a stack of plastic scintillators (range stack) where the kinetic energy and the range of the pions are measured. The range stack is composed of 24 identical azimuthal sectors, each consisting of 21 layers of 1.9 cm-thick plastic scintillation counters. The light from the scintillators is detected by 2 inch photomultiplier tubes (EMI-9954KB) placed at both ends. The light output at each end is approximately 15 photoelectrons per MeV. Two layers of multiwire proportional chambers are interspersed in each sector to measure the axial and the azimuthal positions of the track. The hit positions in the wire chamber were used to improve the range measurement in the online event selection as well as in the offline analysis.

2.5 Photon Detection System

The photon detection system is comprised of barrel and endcap sections. The barrel is segmented in 48 sectors covering 2π in azimuth and ± 95 cm in the beam direction. Each sector consists of 75 interleaved layers of 1 mm lead and 5 mm plastic scintillator, covering 14 radiation lengths. The 75 layers are grouped into 4 radial segments and each of them are viewed at both ends by 3 inch photomultiplier tubes located outside the magnet. The light output is about 10 photoelectrons per MeV. In order to avoid photons escaping through the cracks between the segments, the boundaries of the segments are tilted to be non-projective to the target.

Two endcap photon detectors are installed at the upstream and the downstream ends of the central drift chamber. Each detector consists of 24 azimuthal segments of 66 interleaved layers of 1mm lead and 5 mm scintillator, covering 12.4 radiation lengths. The scintillator layers are oriented perpendicular to the beam axis. Light from the scintillators is absorbed in fast wave-length shifter (BBOT) bars perpendicular to the outer edge of the scintillators viewed through lightguides by 2 inch photomultiplier tubes. The light output is about 10 photoelectrons per MeV, similar to that in the barrel veto. The fraction of visible energy of photons is about 0.3 for both the barrel and endcap photon detection systems.

2.6 Transient Digitizer System

Each transient digitizer[30)] makes a digital record of the waveform of an analog signal from the range stack as a function of time and is used to recognize the decay sequence of $\pi^+ \rightarrow \mu^+ \rightarrow e^+$ in order to identify pions. We have developed 500 MHz transient digitizers with 8-bits dynamic range. The sampling rate of 500 MHz was achieved using two interleaved 250 MHz flash ADC's (Tektronix TKAD508). The memory depth is up to 0.5 msec. For the E787 experiment, a time window of ± 5 μsec with respect the K^+ decay timing was chosen to detect the relatively slow $\mu \rightarrow e$ decay ($\tau_\mu = 2.2$ μsec). The system has zero-suppression capability to reduce the number of data words to be read. The data are read via a FASTBUS

controller with a fast readout time. A typical spectrum of $\pi \rightarrow \mu$ decay observed by the transient digitizer is shown in Fig.8. At present one hundred channels of transient digitizers are used to digitize the range stack signals covering the stopping layers of interest by summing four azimuthally adjacent counters. They are also used in the online μ rejection.

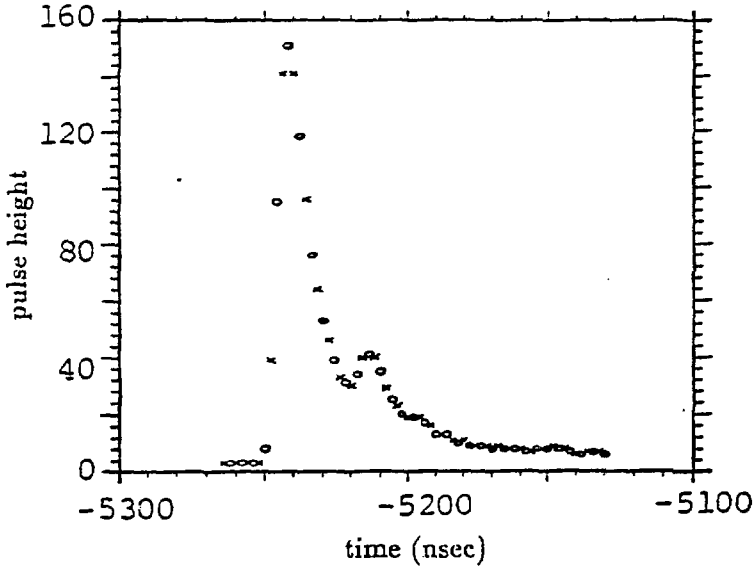

Fig.8 Transient digitizer spectrum of a stopped π followed by $\pi \rightarrow \mu$ decay.

2.7 Data Acquisition System

All counter channels are instrumented with ADCs and TDCs, for the most part LeCroy FERA CAMAC ADCs and pipeline FASTBUS TDCs. The system is based mainly in FASTBUS and the ADC data are read from CAMAC through an ECL bus interface to FASTBUS. A SLAC Scanning Processor (SSP) microprocessor is used as the master in each FASTBUS crate to perform the event selection and to gather and store data in its memory during beam spills.

The trigger system is organized in three levels of increasing complexity. At each trigger stage the reduction of the trigger rate is roughly a factor of 10, to a final trigger rate of about 50−100 events/spill. The first level trigger is based on ECL logic circuits and requires the proper range region for the decay products in the range stack, no energy in the photon veto system and delayed timing with respect to the K^+ stop. The second level uses memory lookup units (MLU) to refine the range of the pions using the information from the target and from the wire chambers in the range stack. In the third level, the SSPs use an algorithm for event selection based on rejection of muons using the transient digitizer information, a cut on the track energy, and a cut on the extra energy in the range stack due to

photon conversion. The data are formatted in the SSP and sent through a CERN FASTBUS Interface (CFI) between beam spills to a MicroVax II host computer.

3. DETECTOR PERFORMANCE

The detector was completed just before the first run in February-May, 1988. This run was devoted mostly to calibration of the subsystems and to trigger studies. During this run approximately 10^{10} stopped K^+ were accumulated for the trigger modes of $K^+ \to \pi^+ \nu\bar{\nu}$, $K^+ \to \pi^+ \mu^+ \mu^-$ and $K^+ \to \pi^+ \gamma\gamma$. The data are presently being analyzed. The performance of the detector, based on these data is described below, focussing on the measurement of range/momentum/energy, the analysis of the transient digitizer data and the photon veto efficiency.

3.1 Range/Momentum/Energy Correlations

The two-dimensional plots in Fig.9 show the correlations between range, momentum and kinetic energy of the charged decay products for a mixed sample of $K_{\mu 2}$ and $K_{\pi 2}$ events. This sample has full acceptance for $K_{\pi 2}$ but only $K_{\mu 2}$ events at large angles satisfy the trigger. Since range and energy-deposit in the target are not corrected for, the peaks of $K_{\mu 2}$ and $K_{\pi 2}$ are shifted and smeared out and results in two distinct bands corresponding to pions and muons. These correlations allow good discrimination of pions from muons in the low energy region.

Fig.10 shows the two-dimensional plots of the total kinetic energy vs. total range and of the total momentum vs. total range for the same mixed sample of $K_{\mu 2}$ and $K_{\pi 2}$, where range and energy in the target are corrected for. It can be seen that the two sharp peaks of $K_{\mu 2}$ and $K_{\pi 2}$ are well separated. The region of interest for $K^+ \to \pi^+ \nu\bar{\nu}$ signals lies between the two peaks.

In Fig.11, the distributions of total momentum, toyal range and total kinetic energy of pions in the $K_{\pi 2}$ samples are shown. Momentum resolution (standard deviation) of $\Delta P/P \sim 2.4\%$, range resolution of $\Delta R/R \sim 1.1$ cm, and energy resolution of $\Delta E/E \sim 3\%$ are obtained, consistent with Monte Carlo estimates.

3.2 Transient Digitizer Analysis

The transient digitizer system is used to distinguish pions from muons by observing the decay sequence of $\pi^+ \to \mu^+ \to e^+$. The π^+ decays with a lifetime of 26 ns into a μ^+ with 4 MeV kinetic energy which in turn decays into e^+ and two ν's with a 2.2 μs lifetime. The endpoint of the e^+ energy is about 50 MeV. The principle of pion identification by the transient digitizers is based on searching for

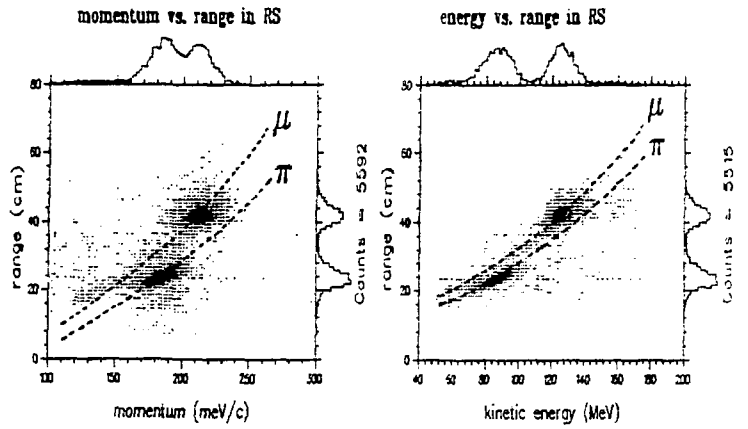

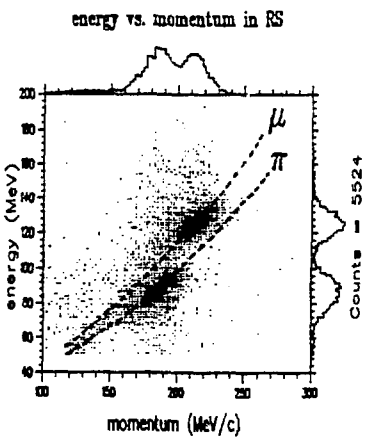

Fig.9 Correlations of momentum, energy, and range for mixed $K_{\pi 2}$ and $K_{\mu 2}$ events. Dashed lines are expected curves for pions and muons.

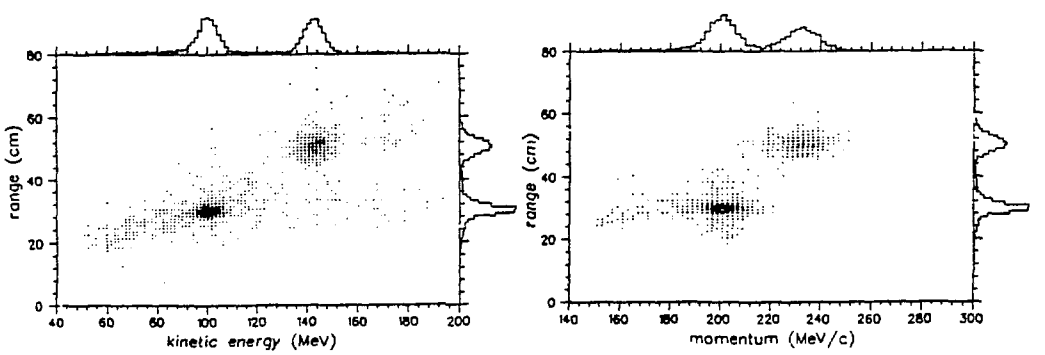

Fig.10 Correlation of total momentum, enery, and range of the events in Fig. 9 after correction for the target.

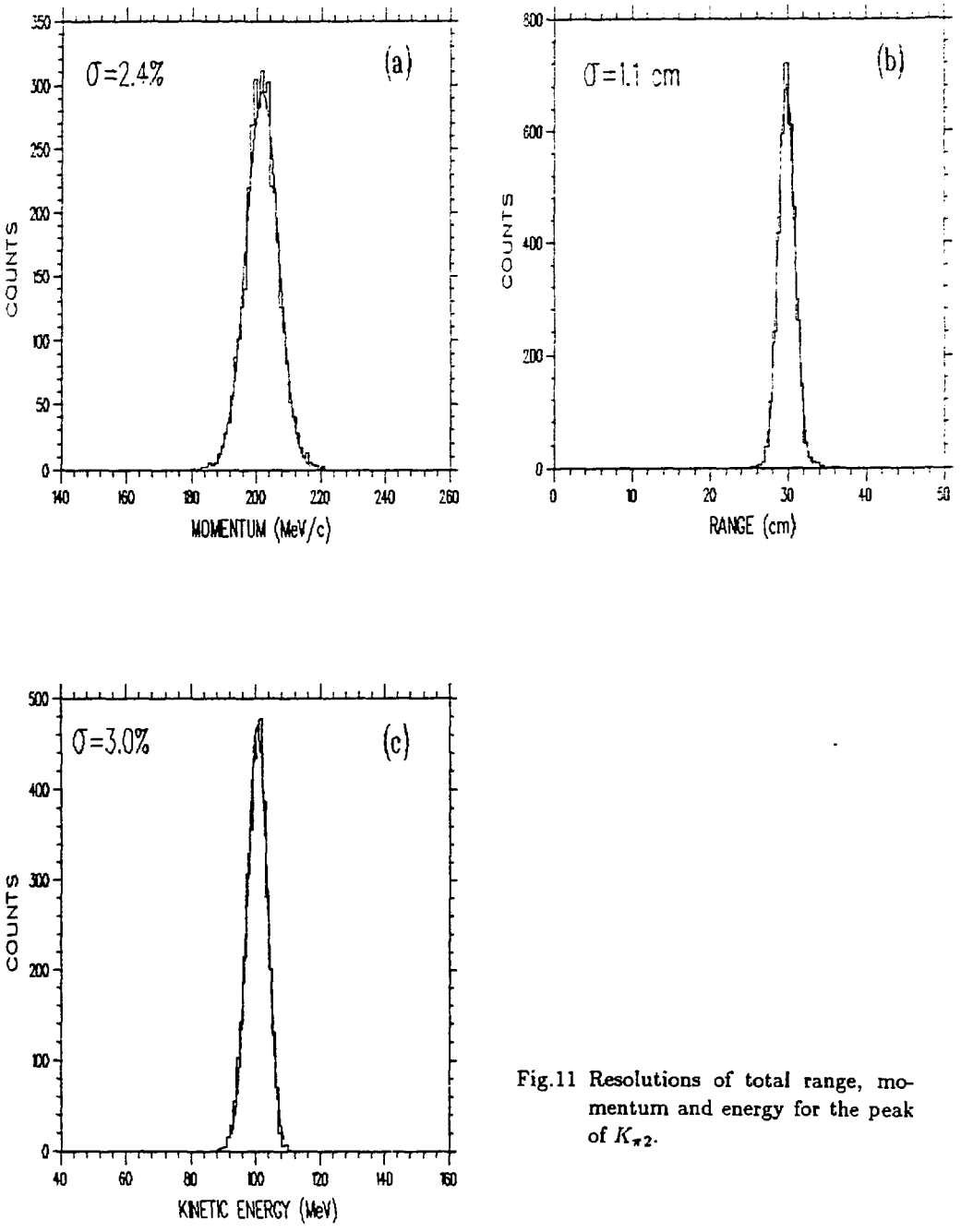

Fig.11 Resolutions of total range, momentum and energy for the peak of $K_{\pi 2}$.

three pulses from the vicinity of the pion stop in the range stack, which satisfy the decay properties (energy and timing) above.

In offline analysis, the identification of the decay of $\pi^+ \rightarrow \mu^+$ is performed by pulse-shape fitting of the transient-digitizer spectrum from the pion stopping counter for a time period up to $\sim$ 150 ns after the pion stop. The pulse-shape fitting to the spectrum is done according to two different hypotheses; the first presumes a single pulse (μ hypothesis) and the second presumes double pulses (π hypothesis). The chi-squares of the two hypotheses are compared to determine whether the second pulse associated with the $\pi \rightarrow \mu$ decay exists. A general minimization program MINUIT was used and the fitting parameters are amplitude and time of each pulse. The template of the pulse shape was determined by averaging the single pulse spectra. Typical examples of the fitting results are shown in Fig.12. The advantage of this approach can be seen in the second event where the second pulse lies on the tail of the first pulse. Since the pion lifetime is 26 ns and the typical pulse width from the scintillator is as much as 20 ns, this kind of event is likely. The time spectrum of μ^+ from π decay is shown in Fig.13, where the second pulse can be found as early as 8 ns from the time of the pion stop. The pion lifetime measured is consistent with the accepted value of 26 ns.

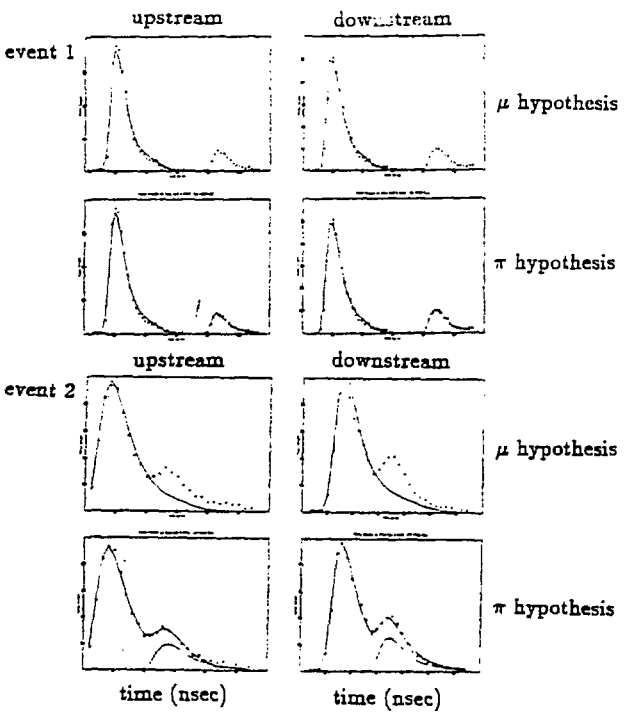

Fig.12 Transient digitizer pulse shape fitting. Two typical events are displayed, where the fitting results of μ hypothesis and π hypothesis are shown for the upstream and downstream ends of the transient digitizer data. Solid lines are fitted curves and dotted lines are data.

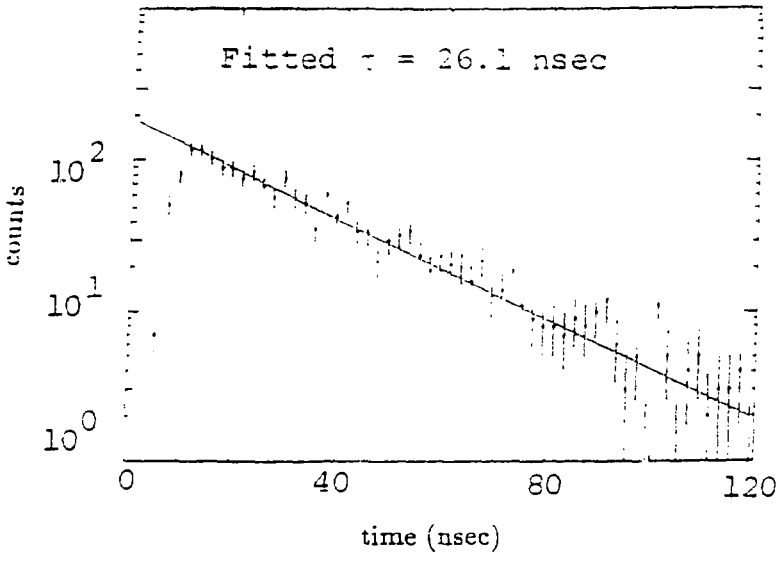

Fig.13 $\pi \rightarrow \mu$ decay time spectra from the transient digitizer data.

In order to reduce accidental backgrounds which simulate the $\pi \rightarrow \mu$ signal. some additional constraints were made on the result of the pulse-shape fitting. Since the muons from the $\pi \rightarrow \mu$ decay are monoenergetic, a useful cut requiring 4 MeV in the second pulse can be made. Typical energy resolution of the second pulse $\sigma \sim 14\%$ is shown in Fig.14(a). The other constraint is related to the spatial position of the muons. Since the range of the muons from the $\pi \rightarrow \mu$ decay is about 1 mm, the spatial position of the muon is the same as that of the pion. In

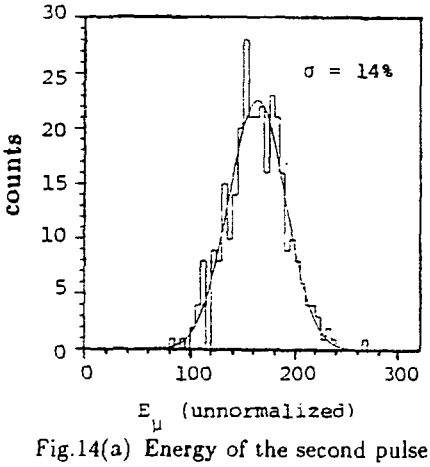

Fig.14(a) Energy of the second pulse from the transient digitizer data.

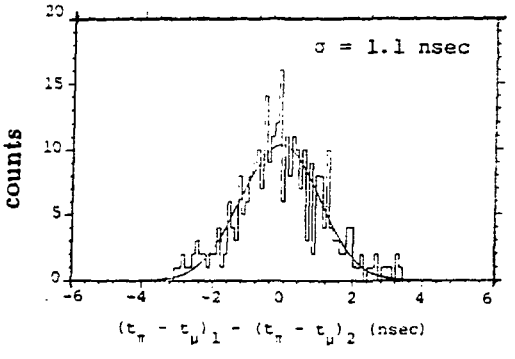

Fig.14(b) Time difference of the first and the second pulse at both end of the pion-stopping counter

order to verify this, the time difference between the first and the second pulse at both ends of the counter (upstream and downstream) are compared: if the second pulse occurs at the position of the pion stop, the time difference at both ends should be equal. The spectrum of the time difference is shown in Fig.14(b), where the mean is located at zero and its standard deviation is about 1.1 ns. Using these constraints, accidentals can be rejected.

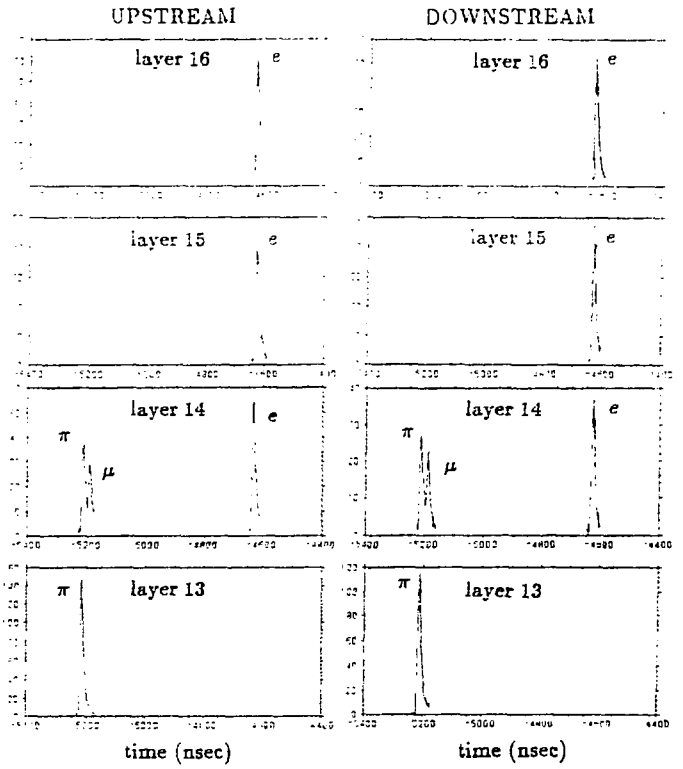

Fig.15 Transient digitizer data of different layers for one typical event. The pion came from the target, passing through the layer 13 and was stopped in the layer 14. The $\pi \rightarrow \mu$ decay was observed in the layer 14. The decay positron from $\mu \rightarrow e$ decay went outwards through the layers 14, 15 and 16.

Fig.15 shows the transient-digitizer spectra of a pion event from several adjacent layers. In the event shown, the pion coming from the target stopped in layer 14 and the second pulse associated with the $\pi \rightarrow \mu$ decay was detected only in layer 14, but not in the adjacent layers. Later, the decay positron from the $\mu \rightarrow e$ decay passed through several layers. The constraints put in the global π recognition are (1) no pulses in adjacent counters at the $\pi \rightarrow \mu$ decay timing, and (2) the starting point of the $\mu \rightarrow e$ decay positron should be in the pion stopping counter. The time spectrum of the $\mu \rightarrow e$ decays thus obtained is shown in Fig.16.

3.3 Photon Veto Inefficiency

The energy resolution of the photon detector was tested by measuring the energy sum of two photons from the decay $\pi^0 \rightarrow \gamma\gamma$ in $K_{\pi 2}$ events. The result is

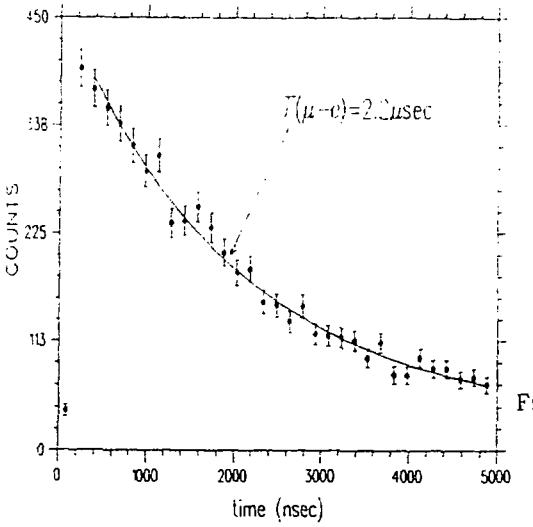

Fig.16 $\mu \to e$ decay time spectra from the transient digitizer data.

shown in Fig.17, where the mean of the distribution agrees well with the total π^0 energy from $K_{\pi 2}$ and a standard deviation of about 38 MeV is obtained. From this, the photon energy resolution is estimated to be $\sigma/E = 8\%/\sqrt{E(\mathrm{GeV})}$.

The total inefficiency for detection of π^0's was measured by comparing the number of $K_{\pi 2}$ events in the momentum spectrum of the $K^+ \to \pi^+ \nu\bar{\nu}$ data with and without the photon veto. The measured inefficiency for π^0 detection, with a threshold of 1 MeV visible energy and the intime requirement of $|t_\pi - t_\gamma| < 10$ ns, is at the level of 5×10^{-6}. This result may lead to a new experimental upper limit on rare π^0 decay, $\pi^0 \to xx'$, where x, x' are non-interacting particles, for which a detailed study is in progress.

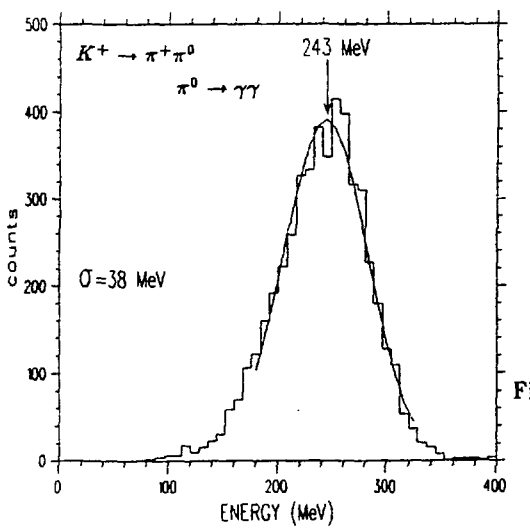

Fig.17 Spectrum of the two photon energy sum for $K_{\pi 2}$ yielding the total energy of the π^0.

4. SUMMARY

The detector for the E787 experiment at Brookhaven National Laboratory has been completed and the first run was taken in 1988. The analysis of the data taken in the 1988 run, which correspond to $\sim 10^{10}$ stopped K^+'s, is now underway to search for $K^+ \to \pi^+ \nu\bar{\nu}$, $K^+ \to \pi^+ \mu^+ \mu^-$ and $K^+ \to \pi^+ \gamma\gamma$ decays.

This research is supported in part by the U.S. Department cf Energy under Contract No. DE-AC02-76CH00016.

References

1) S.L. Glashow, *Nucl. Phys.* **22** (1961) 579; S. Weinberg, *Phys. Rev. Lett.* **19** (1967) 1264; A. Salam, in "*Elementary Particle Theory*" Proc. 8th Nobel Symposium, Aspenäsgarden, 1968, ed. N.Svartholm (Almqvist and Wiksell, Stockholm, 1968)
2) for reviews of rare kaon decays, G.L. Kane and R.E. Shrock, in "*Intense Medium Energy Sources of Strangeness*", Proc. of the Santa Cruz Workshop, 1983, ed. T. Goldman, H.E. Harber and H.F.-W. Sadrozinski (AIP conf. Proc. No.102) p.123; L.S. Littenberg, *Nucl. Phys.* **B279** (1987) 194 ; D.A. Bryman, *Int'l. Journal of Modern Physics*, to be published
3) M.K. Gaillard and B.W. Lee, *Phys. Rev.* **D10** (1974) 897
4) E. Ma and J. Okada, *Phys. Rev.* **D18** (1978) 4219
5) T. Inami and C.S. Lim, *Prog. Theor. Phys.* **65** (1981) 297
6) J. Ellis and J.S. Hagelin, *Nucl. Phys.* **B217** (1983) 189
7) F.J. Gilman and J.S. Hagelin, *Phys. Lett.* **133B** (1983) 443
8) J. Ellis, J.S. Hagelin and S. Rudaz, *Phys. Lett.* **192B** (1987) 201
9) M. Kobayashi and T. Maskawa, *Prog. Theor. Phys.* **49** (1973) 652
10) ARGUS collaboration, H. Albrecht et al., *Phys. Lett.* **192B** (1987) 245; UA1 collaboration, C. Albajar et al., *Phys. Lett.* **186B** (1987) 247
11) W.W. Ash et al., *Phys. Rev. Lett.* **98** (1987) 640
12) H. Albrecht et al., *Phys. Lett.* **209B** (1988) 119
13) R.E. Shrock, in Proc. of the 1982 DPF Summer Study in *Elementary Particle Physics and Future Facilities*, ed. R. Donaldson et al. (1982) P.291
14) U. Türke, *Phys. Lett.* **168B** (1986) 296; G. Eliam, I.L. Hewitt and T.G. Rizzo, *Phys. Lett.* **193B** (1987) 533; W.J. Marciano and Z. Parsa, *Ann. Rev. Nucl. Part. Sci.* (1986) p.171
15) M.K. Gaillard et al., *Phys. Lett.* **123B** (1983) 241; J.F. Nieves and P.B. Pal, *Phys. Rev.* **D32** (1985) 1849; S. Bertoline and A. Masiero, *Phys. Lett.* **174B** (1986) 343
16) F. Wilczek, *Phys. Rev. Lett.* **49** (1982) 1549

17) R.D. Peccei and H.R. Quinn, *Phys. Rev. Lett.* **40** (1978) 233; F.D. Wilczek, *Phys. Rev. Lett.* **40** (1978) 279; L.M. Krause and D.J. Nash, *Phys. Lett.* **B202** (1988) 560
18) G.B. Gelmini and M. Roncadelli, *Phys. Lett.* **99B** (1981) 411
19) M. Lusignoli and A. Pugliese, *Phys. Lett.* **171B** (1986) 468
20) Y. Asano et al., *Phys. Lett.* **107B** (1981) 159
21) J.F. Donoghue, B.R. Holstein and G. Valencia, Phys. ReV. **D35** (1987) 2769
22) G. Ecker, A. Pich and E. de Rafael, *Nucl. Phys.* **B291** (1987) 692
23) G. Ecker, A. Pich and E. de Rafael, *Nucl. Phys.* **B303** (1988) 665
24) Bisi et al., *Nuovo Cim.* **35** (1965) 768; Camerini et al., *Nuovo Cim.* **37** (1965) 1795
25) Y. Asano et al., *Phys. Lett.* **113B** (1982) 195
26) S. Dawson, in Proc. of the 1988 DPF Meetings (1988); S. Raby, G.B. West and C.M. Hoffman, *Los Alomos Preprint* LA-UR-88-2667 (1988), R. Ruskov, *Phys. Lett.* **B187** (1987) 165; T.N. Pham and D.G. Sutherland, *Phys. Rev.* **D34** (1986) 1634; R.S. Willey, *Phys. Rev.* **173B** (1986) 480; R.S. Willey and H.L. Yu, *Phys. Rev.* **D26** (1982) 3287; A.I. Vainshtein, V.I. Zakharov and M.A. Shifman, *Sov. Phys. Usp* **23** (1980) 429; J. Ellis, M.K. Gaillard and D.V. Nanopolous, *Nucl. Phys.* **B106** (1976) 292
27) K.K. Li, in Proc. of the IX Europian Symposium on Antiproton–Proton Interactions and Fundamental Symmetries, Mainz, W. Germany, (1988), to be published
28) J.S. Frank and R.C. Strand, to be published
29) J.V. Cresswell, S. Ahmad, E.W. Blackmore, D.A. Bryman, N. Khan, Y. Kuno and T. Numao, *IEEE*, **NS 35** (1987) 460
30) M. Atiya, M. Ito, J. Haggerty, C. Ng, F.W. Sippach, *IEEE* (1988) to be published.

DISCLAIMER

This report was prepared as an account of work sponsored by an agency of the United States Government. Neither the United States Government nor any agency thereof, nor any of their employees, makes any warranty, express or implied, or assumes any legal liability or responsibility for the accuracy, completeness, or usefulness of any information, apparatus, product, or process disclosed, or represents that its use would not infringe privately owned rights. Reference herein to any specific commercial product, process, or service by trade name, trademark, manufacturer, or otherwise does not necessarily constitute or imply its endorsement, recommendation, or favoring by the United States Government or any agency thereof. The views and opinions of authors expressed herein do not necessarily state or reflect those of the United States Government or any agency thereof.